

This is a postprint version of the following published document:

Martínez-Ratón, Yuri; González-Pinto, Miguel; Velasco, Enrique. (2016). Biaxial nematic phase stability and demixing behaviour in monolayers of rod-plate mixtures. *Physical Chemistry Chemical Physics*. 18(35), pp. 24569-24581.

DOI: <https://doi.org/10.1039/C6CP05022K>

Biaxial nematic phase stability and demixing behaviour in monolayers of rod-plate mixtures

Yuri Martínez-Ratón*

*Grupo Interdisciplinar de Sistemas Complejos (GISC), Departamento de Matemáticas,
Escuela Politécnica Superior, Universidad Carlos III de Madrid,
Avenida de la Universidad 30, E-28911, Leganés, Madrid, Spain*

Miguel González-Pinto†

*Departamento de Física Teórica de la Materia Condensada,
Universidad Autónoma de Madrid, E-28049 Madrid, Spain*

Enrique Velasco‡

*Departamento de Física Teórica de la Materia Condensada,
Instituto de Ciencia de Materiales Nicolás Cabrera
and Condensed Matter Physics Center (IFIMAC),
Universidad Autónoma de Madrid, E-28049 Madrid, Spain*

Abstract

We theoretically study the phase behaviour of monolayers of hard rod-plate mixtures using a fundamental-measure density functional in the restricted-orientation (Zwanzig) approximation. Particles can rotate in 3D but their centres of mass are constrained to be on a flat surface. In addition, we consider both species to be subject to an attractive potential proportional to the particle contact area on the surface and with adsorption strengths that depend on the species type. Particles have board-like shape, with sizes chosen using a symmetry criterion: same volume and same aspect ratio κ . Phase diagrams were calculated for $\kappa = 10, 20$ and 40 and different values of adsorption strengths. For small adsorption strengths the mixtures exhibit a second-order uniaxial nematic-biaxial nematic transition for molar fraction of rods $0 \leq x \lesssim 0.9$. In the uniaxial nematic phase the particle axes of rods and plates are aligned perpendicular and parallel to the monolayer, respectively. At the transition, the orientational symmetry of the plate axes is broken, and they orient parallel to a director lying on the surface. For large and equal adsorption strengths the mixture demixes at low pressures into a uniaxial nematic phase, rich in plates, and a biaxial nematic phase, rich in rods. The demixing transition is located between two tricritical points. Also, at higher pressures and in the plate-rich part of the phase diagram, the system exhibits a strong first-order uniaxial nematic-biaxial nematic phase transition with a large density coexistence gap. When rod adsorption is considerably large while that of plates is small, the transition to the biaxial nematic phase is always of second order, and its region of stability in the phase diagram considerably widens. At very high pressures the mixture can effectively be identified as a two-dimensional mixture of squares and rectangles which again demixes above a certain critical point. We also studied the relative stability of uniform phases with respect to density modulations of smectic, columnar and crystalline symmetry.

PACS numbers: 61.30.Pq,64.70.M-,47.57.J-

*Electronic address: yuri@math.uc3m.es

†Electronic address: miguel.gonzalezp@uam.es

‡Electronic address: enrique.velasco@uam.es

I. INTRODUCTION

It is well known that the properties of biological vesicles and membrane cells strongly depend on their constituent blocks, usually composed of phospholipid bilayers with embedded proteins. These molecules are in general anisotropic (rod or plate-like) and the demixed states usually have liquid-crystal symmetries, such as isotropic (I), nematic (N) or biaxial nematic (B) symmetries. For certain conditions these complex mixtures of biomolecules phase separate, creating regions rich in different species and consequently changing the membrane curvature. There is much experimental evidence of demixing transitions in monolayers and bilayers of mixed anisotropic biomolecules [1–7]. The adsorption of a large variety of mixtures of rod-like molecules in Langmuir monolayers has been extensively studied both experimentally and theoretically. Many of these works focus on the chemical and thermodynamic conditions for which the monolayers become spatially heterogeneous, i.e. when the mixture demixes in different phases usually possessing liquid-crystal ordering [8–11]. Finally many experiments on the adsorption of rod-like colloidal particles at the interfaces separating two immiscible fluids showed the propensity of these particles to self-assemble into clusters of different geometries [12–14]. The degree of adsorption of these particles at the interface and their relative orientation with respect to it strongly depend on their chemical compositions. This in turn can modify their wetting properties and consequently the effective capillary forces acting between particles. The resulting effect is the existence of anisotropy in the pair interaction potential which forces the particles to self-assemble into clusters [13, 15, 16]. When colloids with very different chemical properties are adsorbed at the interface they usually phase separate into phases with different composition of species. A recent experimental work showed how demixing of adsorbed colloids strongly modifies their self-assembling properties [17].

All the systems discussed above share the following properties: (i) they are mixtures of anisotropic particles, (ii) the degrees of freedom of their centres of mass are strongly restricted, usually resulting in an effective two-dimensional fluid, and (iii) the particle axes can rotate in 3D but with certain restrictions which depend on the degree of particle adsorption on the monolayer, bilayer or interface. The main motivation of the present work is the formulation of a very simple model for a binary mixture of anisotropic particles (specifically a mixture of rods and plates) which allows a detailed study of the conditions (particle aspect

ratios, degree of adsorption) under which these mixtures demix into two different phases.

To this purpose we choose particles to have a board-like shape and interact through a hard-core repulsion. Also, for simplicity, we use the Zwanzig approximation to account for the orientational degrees of freedom, which are restricted to be three. Finally, we will use a mean-field density functional (DF) based on the fundamental-measure theory (FMT), derived for the present model in the late 90's [18] and more recently implemented to calculate the phase diagrams of rod and plate board-like particles [19]. Monolayers of one-component rods or plates were recently studied within this theory, considering uniaxial [20] and biaxial [21] particle geometries. In the latter work, phase diagrams were calculated as a function of a geometric parameter $\theta \in [-1, 1]$ that measured particle shape, with $\theta = \pm 1$ for uniaxial rod and plate geometries, respectively. One-component monolayers of prolate or oblate freely-rotating ellipsoids were also recently studied via the Parsons-Lee DF and Molecular-Dynamics simulations [22]. In particular, the effect of orientational restriction of ellipsoids on the orientational properties of monolayers was studied. The ground states of monolayers of hard ellipsoids interacting through a quadrupole pair-potential were recently found [23]. Apart from the T-like configurations, three more particle orientations were predicted to be stable.

Stable B phases were observed in 3D lyotropic fluids [24] and also in liquid-crystals made of bent-core organic molecules [25–28]. However, in the latter case controversial issues about the correct identification of the B phase still remain. Recent experiments on colloidal dispersions of board-like mineral biaxial particles showed an stable B phase in some range of particle aspect ratios [29] while the degree of biaxiality can be tuned by an external magnetic field [30]. For recent reviews on B liquid-crystals see Refs. [31–33]. As we have already shown in previous works [20–22] the 2D constraint on the centers of mass of plates favors the stability of the B phase. We will show here that the same constraint together with a high adsorption of rods greatly enhance the stability of the B phase in rod-plate mixtures.

Here we extend our previous model [20] to a binary mixture of uniaxial rods and plates. Board-like-shaped rods and plates are taken to be symmetric: although they have different eccentricities (prolate and oblate), their volumes and their aspect ratios (ratio between major and minor particle edge-lengths) are taken to be the same. This choice of shape geometries is motivated by their extensive use in studies of the biaxial-nematic (B) phases stability with respect to nematic-nematic (N-N) phase separation in binary [34–36] and polydisperse

[37, 38] mixtures of rods and plates. We are interested in the effect of particle adsorption on the phase behaviour of the mixture, in an effort to elucidate (i) the propensity of the system to phase separate into different phases, (ii) the nature (second vs. first order) of the N-B transition when the adsorption strengths are changed, (iii) the relative stability of the B phase with respect to the N or other non-uniform phases, and (iv) the representative phase diagrams of the system (calculated for certain selected values of model parameters). In general we found a rich phase behaviour with the presence of two disconnected demixed N-B phase transitions, one located at low pressures, with a B phase rich in rods, and the other at very high pressures, with a B phase rich in plates (although B-B demixing also occurs in a narrow range of pressures). When plates are strongly adsorbed, the mixture exhibits a strong first-order phase transition. Different demixing scenarios depend on the relative values of plate and rod adsorption coefficients. When adsorption of rods is large while that of plate is small, the B-phase stability is greatly enhanced, the N-B transition is always of second order, and no demixing occurs.

The article is organized as follows. In Sec. II we introduce the model and the theoretical tools used to perform the calculations. In Sec. III we summarize all the results obtained, with subsections presenting different mixtures with various relative adsorption strengths and particle aspect ratios. Finally some conclusions are drawn in Sec. IV.

II. MODEL

We use the Zwanzig model for a binary mixture of prolate (rods) and oblate (plates) board-like particles with centres of mass lying on the xy plane and with main axes pointing along the $\nu = x, y, z$ directions. The edge lengths of species s ($s = 1$ for rods and $s = -1$ for plates) are represented through the tensor

$$\sigma_{s\nu}^\tau = \sigma_s + (L_s - \sigma_s) \delta_{\nu\tau}, \quad (1)$$

with $\delta_{\nu\tau}$ the Kronecker delta symbol, while L_s and σ_s are the particle sizes parallel and perpendicular to the main particle axis, respectively. Therefore, particles are uniaxial parallelepipeds with a square section of area σ_s^2 . Only symmetric mixtures will be studied, namely those composed of particles with the same volume (which is set to unity, $v_0 = L_s \sigma_s^2 = 1$), and with aspect ratios κ_1 and κ_{-1} related by $\kappa \equiv \kappa_1 = L_1/\sigma_1 = \kappa_{-1}^{-1} = \sigma_{-1}/L_{-1} \geq 1$. Thus

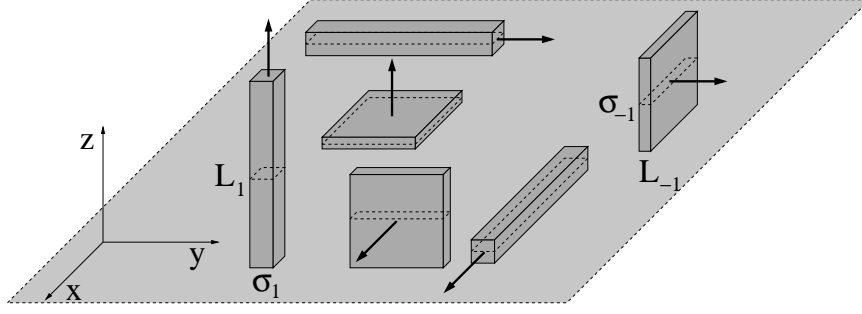


FIG. 1: Schematic representation of the Zwanzig model of a symmetric rod-plate mixture adsorbed on a monolayer.

the edge lengths of the different species are calculated as $L_s = \kappa^{2s/3}$, $\sigma_s = \kappa^{-s/3}$. See Fig. 1 for a schematic representation of our model.

The theory used in the present calculations is the uniform limit of the FMT density functional obtained by applying the dimensional crossover property. This feature allows to correctly transform the functional from 3D to 2D by assuming a 3D density profile, for species s and orientation along the ν -axis, of the form $\rho_{s\nu}^{(3D)}(\mathbf{r}) \equiv \rho_{s\nu}\delta(z)$, i.e. imposing that the particle centres of mass are constrained to the flat surface perpendicular to z . When this density is substituted into the 3D version of the excess free-energy functional, the resulting functional depends on the (constant) 2D number densities

$$\rho_{s\nu} = \rho x_s \gamma_{s\nu}, \quad (2)$$

where ρ is the total number density, x_s is the molar fraction of species s , while $\gamma_{s\nu}$ is the fraction of species s with main axes pointing along the ν -direction. Obviously these quantities fulfill the following constraints: $\sum_s x_s = 1$ and $\sum_\nu \gamma_{s\nu} = 1$ or alternatively $\sum_s \rho_s = \rho$ and $\sum_\nu \rho_{s\nu} = \rho_s$, with $\rho_s = \rho x_s$ the number density of species s . The resulting excess free-energy density in reduced thermal units kT depends on the following weighted densities:

$$n_0 = \rho = \sum_{s,\nu} \rho_{s\nu}, \quad n_2 = \eta = \sum_{s,\nu} \rho_{s\nu} \sigma_{s\nu}^x \sigma_{s\nu}^y, \quad (3)$$

$$n_{1x} = \sum_{s,\nu} \rho_{s\nu} \sigma_{s\nu}^x, \quad n_{1y} = \sum_{s,\nu} \rho_{s\nu} \sigma_{s\nu}^y, \quad (4)$$

and has the explicit form

$$\Phi_{\text{exc}} \equiv \frac{\beta \mathcal{F}_{\text{exc}}}{A} = -n_0 \log(1 - n_2) + \frac{n_{1x} n_{1y}}{1 - n_2}, \quad (5)$$

where $\beta = 1/kT$ is the Boltzmann factor and A the total area of the system. We note that the weighted density n_2 is just the total packing fraction, η , of the binary mixture. The ideal part, $\Phi_{\text{id}} \equiv \beta\mathcal{F}_{\text{id}}/A$ is, as usual

$$\Phi_{\text{id}} = \sum_{s,\nu} \rho_{s\nu} (\log \rho_{s\nu} - 1), \quad (6)$$

and the effective interaction between species s , with projected area on the xy plane $a_{s\nu} = \sigma_{s\nu}^x \sigma_{s\nu}^y$, and the surface, is accounted for by an external potential contribution to the free-energy density:

$$\Phi_{\text{ext}} \equiv \frac{\beta\mathcal{F}_{\text{ext}}}{A} = - \sum_{s\nu} \epsilon_s \rho_{s\nu} a_{s\nu}. \quad (7)$$

Note that this contribution is proportional to the projected particle areas, and that we allow for the possibility that the adsorption strengths $\epsilon_s \geq 0$ be dependent on species s .

To find the equilibrium orientational properties of the fluid we minimize the total free-energy density $\Phi = \Phi_{\text{id}} + \Phi_{\text{exc}} + \Phi_{\text{ext}}$ with respect to the fractions $\gamma_{s\nu}$. These can be related to the uniaxial nematic order parameters,

$$Q_s \equiv \frac{3\gamma_{sz} - 1}{2}, \quad s = \pm 1, \quad (8)$$

which measure the order about the direction perpendicular to the surface, and to the biaxial nematic order parameters,

$$\Delta_s = \frac{s(\gamma_{sx} - \gamma_{sy})}{\gamma_{sx} + \gamma_{sy}}, \quad s = \pm 1, \quad (9)$$

which measure the degree of biaxial order. Note that the factor $s = \pm 1$ in the definition of Δ_s is necessary to take account of the orthogonality of the plate and rod main axes when their projections have the same orientations.

We have calculated the phase diagram by searching for possible demixing transitions through (i) the equality between chemical potentials of species s , $\beta\mu_s \equiv \frac{\partial\Phi}{\partial\rho_s}$, and (ii) the equality between the pressures of the demixed phases. The latter can be calculated as

$$\beta p = \frac{n_0}{1 - n_2} + \frac{n_{1x}n_{1y}}{(1 - n_2)^2} \quad (10)$$

(in reduced thermal units). These calculations are equivalent to finding the coexisting molar fractions of the demixed phases through the double-tangent construction of the Gibbs free-energy density,

$$\beta g(x) \equiv \Phi + \beta p \rho^{-1}, \quad (11)$$

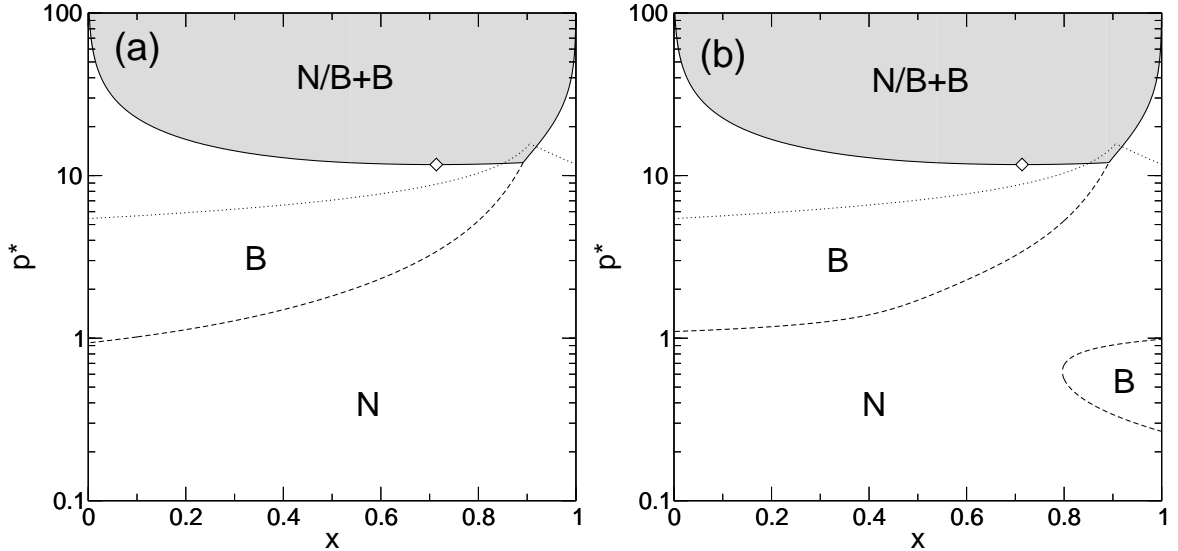


FIG. 2: Phase diagrams of rod-plate binary mixtures with $\kappa = 10$ shown in the pressure-molar fraction of rods ($x \equiv x_1$) plane. The values of the external potential strengths in (a) and (b) are $(\epsilon_1, \epsilon_{-1}) = (0, 0)$ and $(1, 1)$, respectively. The dashed lines show the second order N-B transitions, while the solid lines show the binodals of N-B or B-B coexistences. The grey-shaded region (labelled as N/B+B) is the demixing region. The open diamond corresponds to the demixing critical point. The dotted lines are the spinodal instability to non-uniform phases. The regions of stability of the N and B phases are correspondingly labelled.

as a function of the molar fraction $x \equiv x_1$ at constant value of p . This constraint allows us to find the total number density $\rho(x, p)$ as a function of x at fixed p , while all the quantities $\gamma_{s\nu}$ should be calculated for the same values (x, p) from the set of equations $\partial\Phi/\partial\gamma_{s\nu} = 0$. To find the location of second-order phase transitions to biaxial phases we use a bifurcation analysis of the total free-energy density Φ with respect to the (small) order parameters Δ_s . For details of these calculations see Appendix A. In the rest of the manuscript we use dimensionless densities $\rho^* \equiv \rho v_0^{2/3}$ and pressures $p^* \equiv \beta p v_0^{2/3}$.

III. RESULTS

This section is devoted to the study of the phase diagram topologies as a function of the adsorption strengths $(\epsilon_1, \epsilon_{-1})$ and the aspect ratio κ of the mixture.

A. Mixtures with $\kappa = 10$ and low and symmetric adsorption

We firstly studied the monolayer of rods and plates with zero adsorption to the surface by setting $(\epsilon_1, \epsilon_{-1}) = (0, 0)$. The phase diagram obtained for a mixture with $\kappa = 10$ is shown in Fig. 2(a) in the pressure-composition plane. The dashed line, which departs at its lowest pressure from the left vertical axis ($x \equiv x_1 \sim 0$), represents a continuous N-B phase transition.

From low to high pressures, but below the N-B spinodal, the configuration of plates changes from a nearly equimolar composition of their three species to that in which the species with the largest (square) projected area, equal to $\kappa^{2/3}$, has the lowest composition while the other two species, with rectangular projected shapes of aspect ratio κ and surface area $\kappa^{-1/3}$, have equal compositions. The plate axes of the latter species are parallel to the surface but their rectangular sections are yet randomly oriented in 2D. This phase is a planar N with a negative uniaxial order parameter which decreases with pressure. The configuration of rods at low pressures always exhibits a preferential alignment perpendicular to the monolayer, resulting in a higher proportion of projected (small) squares of surface area $\kappa^{-2/3}$. The other two species of rods, having rectangular shapes, aspect ratio κ , and surface area $\kappa^{1/3}$, have again the same composition. Thus the uniaxial order parameter of rods is always positive and increases with pressure. The authors of the recent work [39] showed that the uniaxial order parameter Q_1 of one-component rods on a surface increases linearly from zero as a function of ρ^* .

As the pressure increases, the fraction of plates with their axes oriented parallel to the surface and that of rods oriented perpendicular to it become larger, and the uniaxial order parameters tend to $-1/2$ and 1 , respectively. At a certain pressure (which depends on molar fraction), the xy orientational symmetry is broken in a continuous fashion, and the projected rectangular species for both, rods and plates, begin to align along a preferential direction, say the y direction. From this pressure the B phase becomes stable and the B order parameters continuously increase from zero. See Fig. 3 for a sketch of projected shape configurations for the different phases. Fig. 2 indicates that biaxial ordering is promoted by the plates: the N-B spinodal, departing from the left vertical axis ($x \equiv x_r = 0$), is a monotonically increasing function of x and possesses an asymptote at $x = 1$. The latter means that one-component monolayers of rods do not exhibit B ordering. From now on we

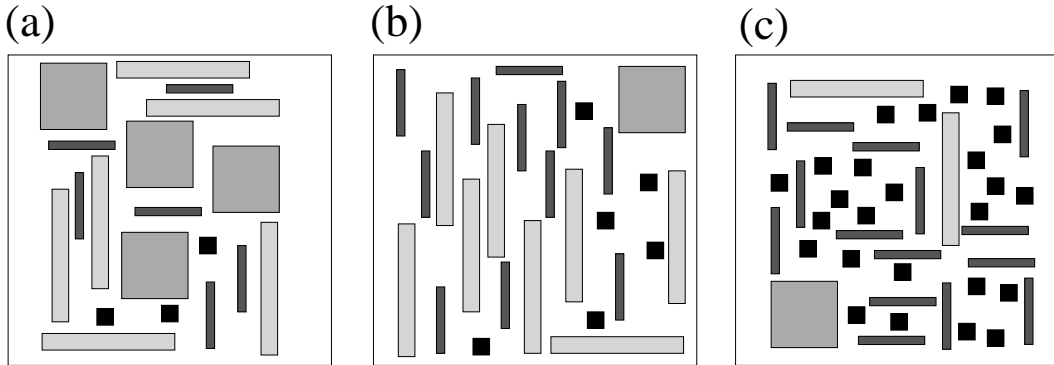


FIG. 3: Schematic representation of projected particle areas corresponding to rod-plate binary mixtures in (a) a low-density N phase, (b) an intermediate-density B phase, and (c) a high-density N phase.

refer to this spinodal as the *plate N-B spinodal*.

At very high pressures, most of the plate axes align parallel to the monolayer, while those of rods are perpendicular to it. Thus the system can be approximated by a 2D mixture of Zwanzig hard rectangles (of area $\kappa^{-1/3}$ and aspect ratio κ) and parallel hard squares (of area $\kappa^{-2/3}$). This 2D mixture demixes into two phases, each one rich in one of the species, as shown in Fig. 2. The critical point of the demixing transition is above the N-B spinodal, meaning that B-B coexistence takes place in some pressure interval. For pressures above the crossing point between the right demixing binodal and the N-B spinodal the system phase separates into a B phase, rich in plates, and a N phase, rich in rods. Finally the dotted line in Fig. 2 represents the spinodal instability of the uniform phases with respect to density modulations, which corresponds to the presence of stable non-uniform phases (see Appendix B for details on these calculations). We can see that the N/B-B demixing is, except for a small interval of pressures, metastable with respect to transitions to non-uniform phases.

Fig. 2 (b) shows the phase diagram when the adsorption strengths are still relatively small: $(\epsilon_1, \epsilon_{-1}) = (1, 1)$. We can observe that the phase diagram topology is similar to that of the preceding case, except that now there appears a region, close to $x = 1$ and bounded by a dashed line, where the B phase becomes stable. From now on this spinodal will be called the *rod N-B spinodal*. The total free-energy is lowered when the fraction of rods with main axes parallel the monolayer increases, since this is proportional to the projected areas. In turn, these rods exhibit two continuous N-B and B-N transitions: B

ordering increases with pressure, reaches a maximum, then decreases and finally disappears altogether. This reentrant behaviour of the B phase with pressure can be explained as follows. When the loss in free-energy given by a preferential adsorption and further alignment of rods with projected rectangular shapes cannot compensate the free-energy increase due to the large excluded volumes between rectangular projected species, as compared to those of small squared species, the most favored configuration of particles is that of rods pointing perpendicular to the monolayer. As the total amount of rods lying on the surface becomes small a B-N transition takes place. This behaviour was already found in monolayers of one-component Zwanzig rods with $\kappa > \kappa_c$ and zero adsorption. The values of κ_c were found to be 21.3 and 12 from the spatially continuous [20] and discrete lattice models [39]. When the continuous orientational degrees of freedom are restored, this transition disappears [22]. However if particles can rotate freely except for a small solid angle with respect to the surface normal, the B phase again becomes stable [22]. Thus in real situations when the surface/interface promotes a preferential adsorption of rods with their axes parallel to the surface the B phase will certainly become stable.

B. Mixtures with $\kappa = 10$ and high and symmetric adsorption

Now we proceed to describing the phase behaviour of monolayers of rods and plates with relatively high adsorption strengths, specifically those with $(\epsilon_1, \epsilon_{-1}) = (4, 4)$. The phase diagram in the pressure-composition and total density-composition planes are shown in Fig. 4(a) and (b), respectively. The most salient features that can be observed from the figure are: (i) the presence of strong N-B demixing at pressures located between two tricritical points, both lying on the rod-N-B spinodal which ends at $x = 1$, and (ii) the existence of a strong first order N-B transition departing from $x = 0$ and ending in a tricritical point located at the plate-N-B spinodal. Panel (b) shows the density of the coexisting phases along all these binodals and spinodals.

We first describe the N-B demixing. Fig. 4(b) shows that the values of the coexisting densities in the demixed phases are similar, with B being the densest phase, rich in rods (two different pairs of coexisting densities are shown with circles and squares). However the packing fraction has the opposite behaviour (see the black line of Fig. 5): the phase with the highest packing fraction is the N phase, rich in plates. This behaviour (nearly the same

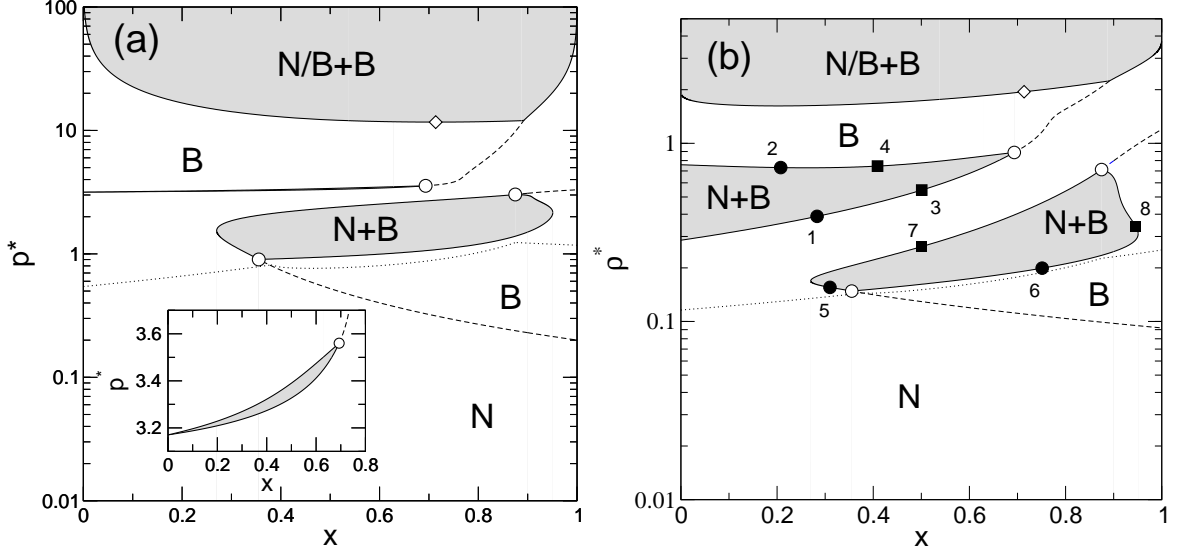


FIG. 4: Phase diagrams of rod-plate binary mixtures for $\kappa = 10$ and $(\epsilon_1, \epsilon_{-1}) = (4, 4)$ in the (a) pressure-molar fraction plane, (b) scaled density-molar fraction plane. Solid lines show the binodals of N-B (or B/B) coexistence, with the coexistence regions shaded in grey. The dashed, dotted lines and diamond have the same meaning as in Fig. 2. Open circles correspond to tricritical points, while black squares and circles in (b) are used to show a pair of coexisting points at different binodals. Inset in (a) is a zoom showing the first-order character of the N-B transition.

coexisting densities but very different composition) is typical in entropy-driven demixing. Note that plates in both coexisting N and B phases have always a positive uniaxial order parameter along the binodals [see Fig. 6(b)], so the fraction of projected large squares (cross-section of plates) is relatively high. The projected rectangles corresponding to rods lying on the surface also have a relatively high fraction (see the negative values of Q_1 in (a) along the binodals, except for a region close to the upper tricritical point), as compared to that of the square projected areas (when rods point perpendicular to the monolayer). As usually occurs in entropy-driven demixing, the total excluded area between the rod-projected rectangles and the plate-projected squares is lowered if the demixed phases are rich in one of the species. The high proportion of large squares is the reason behind the high packing fraction values of the coexisting N phase, as compared to that of the B phase. It is interesting to note the highly non-monotonic behaviour of the packing fraction along the demixing binodals (see Fig. 5), a direct consequence of the dependence of η not only on ρ^* and x but also on the order parameters Q_s . Finally Fig. 7 shows the evolution of the biaxial order parameters

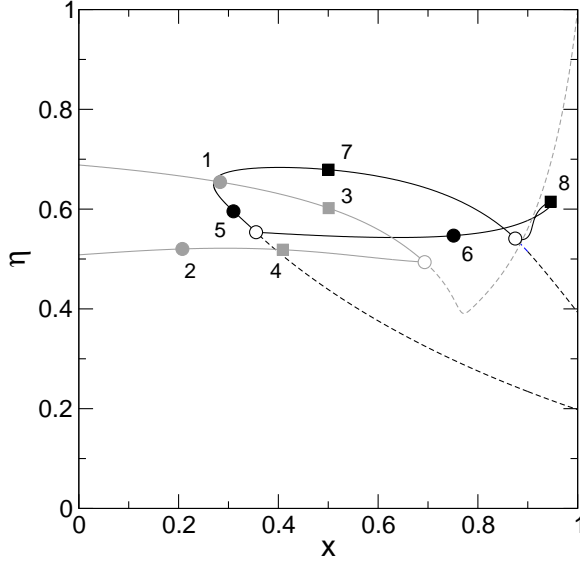


FIG. 5: Packing fractions corresponding to the N-B coexistence binodals (solid) and N-B second-order transitions (dashed) of a rod-plate binary mixture with $\kappa = 10$ and $(\epsilon_1, \epsilon_{-1}) = (4, 4)$ as a function of molar fraction. The symbols have the same meanings as in Fig. 4 and correspond to the same state points. Packing fractions corresponding to the lines belonging to the low pressure N-B demixing and to the strong first order N-B transition of Fig. 4(b) are here shown in grey and black, respectively.

along the demixing binodals. The biaxial order of both species along the coexisting B phase rapidly increases and saturates to its highest value (unity) as the mixture gets away from the lower tricritical point. At some point they invert their monotonicity and decrease to zero at the upper tricritical point.

From the other side of the phase diagram ($x = 0$), and for intermediate values of pressure, a strong first order N-B phase transition takes place, as can be inferred from the large coexisting density gap in Fig. 4(b). This transition ends in a tricritical point located at the plate-N-B spinodal, and is driven by the reorientation of plates. Note the positive and negative values of Q_{-1} , corresponding to the coexisting N and B phases, respectively [see Fig. 6(b)]. The rods are now mainly oriented perpendicular to the monolayer (perfectly oriented in the N phase, and with a small degree of orientation in the B phase). It is interesting to note that the coexisting molar fractions are now similar (with the B phase slightly rich in plates), while the coexisting densities are very dissimilar (B being the densest phase). This transition is driven by a differential change in free-energy from a N phase with

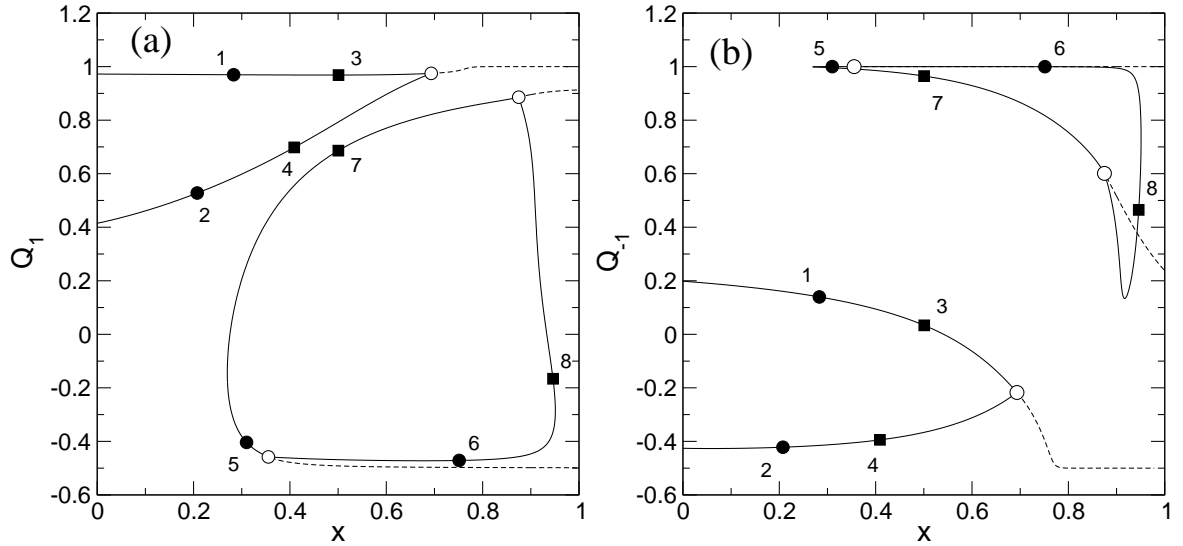


FIG. 6: Uniaxial orientational order parameters of (a) rods, and (b) plates as a function of the molar fraction along the N-B coexisting binodals and spinodals of Fig. 4, i.e. for a rod-plate binary mixture with $\kappa = 10$ and $(\epsilon_1, \epsilon_{-1}) = (4, 4)$. The solid and dashed lines, and symbols (showing the same state points) have the same meanings as in Fig. 4.

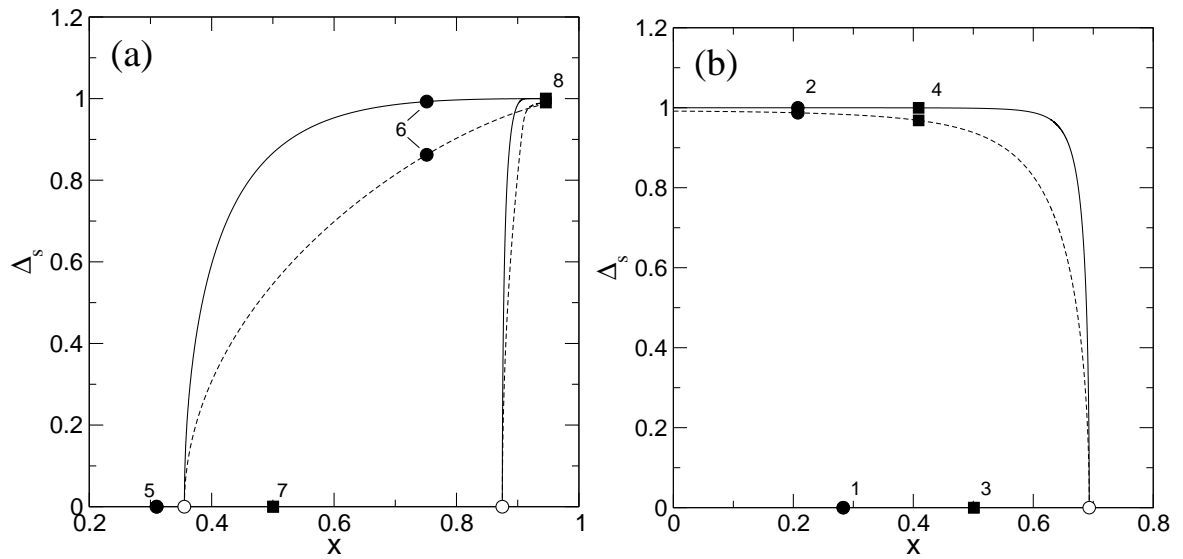


FIG. 7: Biaxial orientational order parameter of rods (solid) and plates (dashed) as a function of the molar fraction along the N-B demixing binodals (a) and along the N-B strong first order transition (b) corresponding to Fig. 4, i.e. for the rod-plate binary mixture with $\kappa = 10$ and $(\epsilon_1, \epsilon_{-1}) = (4, 4)$. The symbols have the same meanings as in Fig. 4 and represent the same state points.

a high fraction of adsorbed large squares (plate axes perpendicular to the monolayer) to a B phase with a high fraction of projected rectangles (corresponding to plates with their axes lying on the monolayer and pointing along y). When we follow a constant pressure path from the N to the B coexisting phases, the free-energy contribution corresponding to the external potential increases, while that coming from the entropic interaction part is lowered (because the particle excluded areas decrease). The differential change in the total adsorbed area of particles is huge, so the transition becomes strongly first order. Again the coexisting packing fractions are inverted: that of the B phase is lower (see the gray solid curve in Fig. 5). At very high pressures the same N/B-B demixing transition ending in a critical point takes place [similar to the cases $(\epsilon_1, \epsilon_{-1}) = (0, 0)$ and $(1, 1)$].

Finally we calculated the instability of uniform phases with respect to non-uniform density modulations. The pressures and densities at which these instabilities occur are plotted as a function of x in Fig. 4(a) and (b), respectively. We can see that the lower tricritical point is located above this curve, suggesting that all demixing transitions are metastable with respect to transitions or demixing between non-uniform phases. When the molar fraction of plates with axes perpendicular to the surface is high due to their large surface adsorption, their square cross-sections may crystallize in a simple square lattice at a certain pressure. If pressure is increased beyond this value, plates will reorient their axes parallel to the monolayer and consequently crystal ordering could be destabilized with respect to a uniform or nonuniform phase exhibiting B ordering. On the other side of the phase diagram, where the molar fraction of rods is high and the B phase is stable, the most likely scenario is that of B-smectic or B-columnar phases, where the projected rectangles exhibit two-dimensional smectic or columnar arrangements. These open questions should be settled out by performing DF minimisation with respect to non-uniform density profiles, $\rho_{sv}(x, y)$, and search for possible coexistences, a formidable task that we leave for future studies.

C. Mixtures with $\kappa = 10$ and asymmetric adsorption

In this section we study the effect of adsorption asymmetry on the phase behaviour of monolayers of rods and plates. To this purpose we have chosen the adsorption strengths as $(\epsilon_1, \epsilon_{-1}) = (5, 3)$, i.e. rods are more strongly adsorbed on the surface than plates. To better compare the results obtained with those described in the preceding sections, we

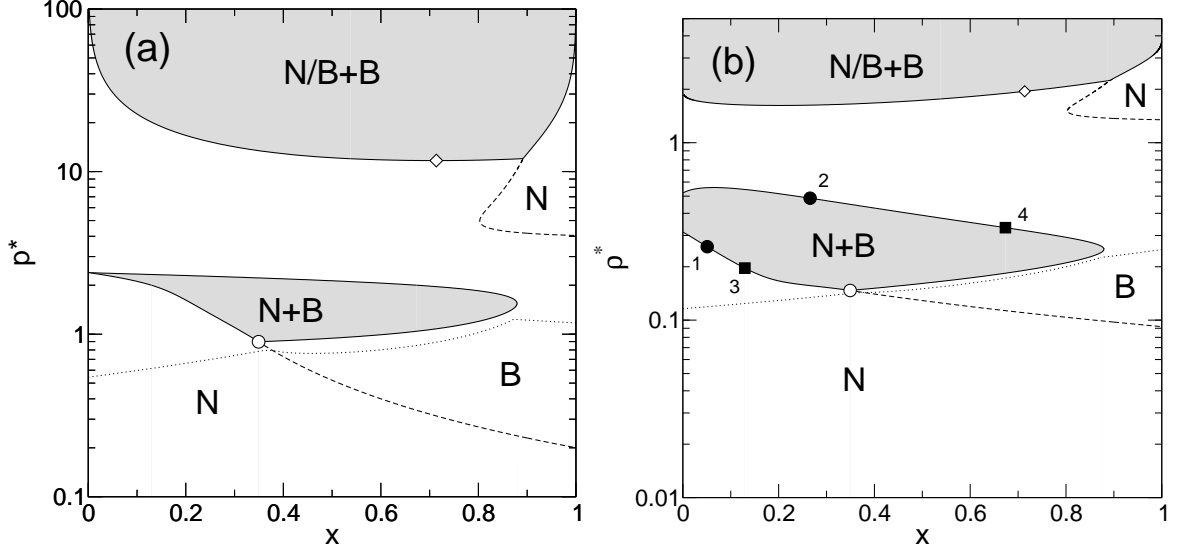


FIG. 8: Phase diagrams in the pressure-molar fraction [(a)] and scaled density-molar fraction [(b)] planes for a rod-plate binary mixture with $\kappa = 10$ and $(\epsilon_1, \epsilon_{-1}) = (5, 3)$. The lines, symbols and labels have the same meanings as in Fig. 4.

again set the aspect ratio to $\kappa = 10$. The phase diagram for this mixture is plotted in Fig. 8 in the (a) pressure-composition and (b) density-composition variables. The main features we can extract from these results are: (i) When the rods are strongly adsorbed on the surface, the lower part of the rod-N-B spinodal meets the plate-N-B spinodal at intermediate compositions, creating a monotonic, fully connected spinodal curve over the whole composition interval. (ii) There is a lower tricritical point located on this curve, above which a demixing transition occurs. (iii) The demixing transition coalesces with the strong first-order transition driven by plates at higher pressures (the one ending at $x = 0$). (iv) The upper part of the rod-N-B spinodal joins the right part of the plate-N-B spinodal, creating an island of N phase stability. (v) The entropic N/B-B demixing at high pressure remains invariant, which confirms the fact that the system behaves like a 2D mixture of squares and rectangles. Fig. 9 shows the strong non-monotonic behaviour of the packing fraction along the coexistence binodals, with the presence of a large loop. (vi) The spinodal for the uniform phase instability with respect to density modulations is located again below the tricritical point. Also, packing fraction inversion (with respect to density) does occur, with N being the densest phase. Figs. 10(a) and (b) show the uniaxial order parameters along the binodals, with a B phase of rods and plates having axes lying on the monolayer,

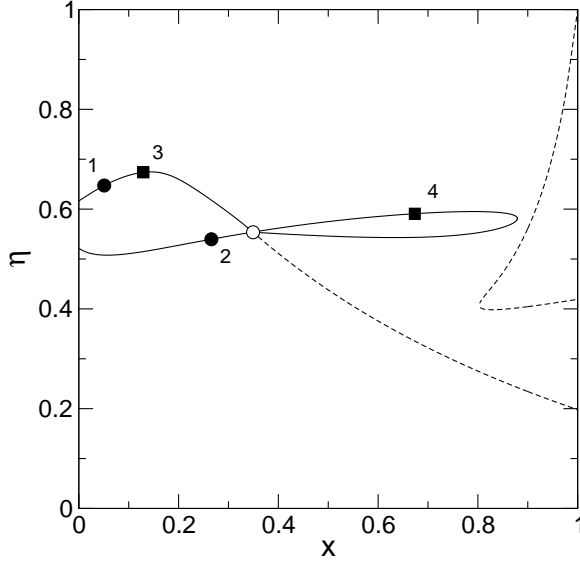


FIG. 9: Packing fraction, as a function of the molar fraction, along the N-B binodals and spinodals of Fig. 8, i.e. for the rod-plate mixture with $\kappa = 10$ and $(\epsilon_1, \epsilon_{-1}) = (5, 3)$. The lines and symbols have the same meaning as in Fig. 8, and they correspond to the same state points.

and a N phase with plate axes pointing perpendicular to it. Interestingly, the rods in N phase are oriented parallel to the surface, although to a lesser degree. The insets show the completely saturated ordering of particles (perpendicular and parallel to the surface for rods and plates, respectively) along the boundaries limiting the island of N phase stability. Finally Fig. 11 shows the biaxial order parameters along the coexisting binodals, which have the usual behaviour: a rapid increase as the system gets away from the tricritical point, and then saturation to perfect biaxial ordering.

Fig. 12(a) shows the phase diagram of a mixture with $\kappa = 10$, but with larger asymmetry in their adsorption strengths, $(\epsilon_1, \epsilon_{-1}) = (5, 1)$. Now the plates are slightly adsorbed on the surface, while rods are strongly adsorbed. We can see that: (i) the demixing and first-order N-B transitions (present in the $(5, 3)$ -mixtures) are substituted by continuous transitions, with the N-B spinodal now being a monotonically decreasing function of x . Thus the region of B stability is greatly enhanced. (ii) The island of N-phase stability and the N/B-B demixing at high pressure remain as before. Fig. 12(b) shows the phase diagram of the mixture $(\epsilon_1, \epsilon_{-1}) = (2, 5)$, i.e. plates and rods are strongly and slightly adsorbed, respectively. Note the presence of a strong first-order N-B transition driven by the desorption of plates at intermediate pressures. As before, this transition ends in a tricritical point located on the

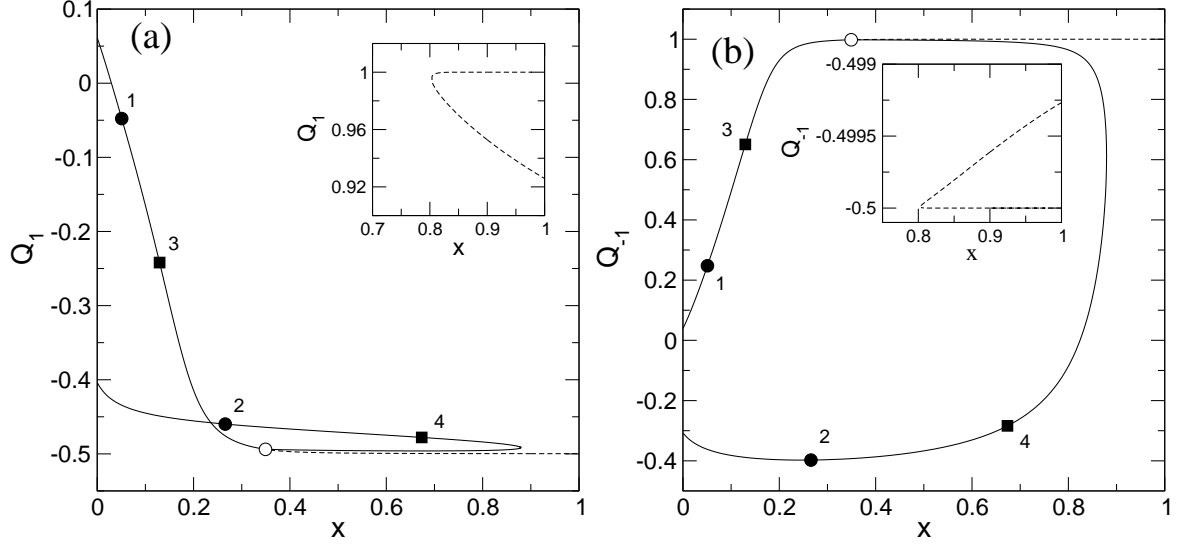


FIG. 10: Uniaxial nematic order parameter of (a) rods, and (b) plates along the B binodals and spinodals of Fig. 8, i.e. for the rod-plate binary mixture with $\kappa = 10$ and $(\epsilon_1, \epsilon_{-1}) = (5, 3)$. The lines and symbols have the same meaning as in Fig. 8. The inset in (a) shows the order parameter corresponding to the highly oriented rods along the N-B spinodal located at high pressures and close to $x = 1$ in Fig. (8). The inset in (b) shows the order parameter of plates with close-to-perfect planar nematic ordering along the same N-B spinodal.

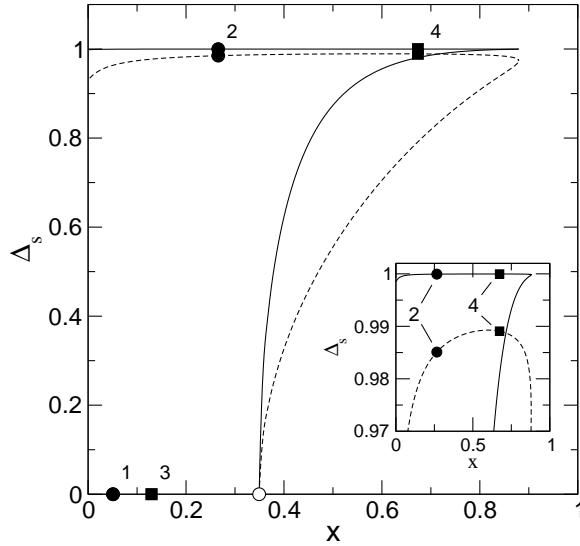


FIG. 11: Biaxial orientation order parameter of rods (solid curve) and plates (dashed curve) along the B binodals of Fig. 8, i.e. for a rod-plate binary mixture with $\kappa = 10$ and $(\epsilon_1, \epsilon_{-1}) = (5, 3)$. The symbols have the same meaning as in Fig. 8, and show the same state points. The inset is a zoom of the main figure.

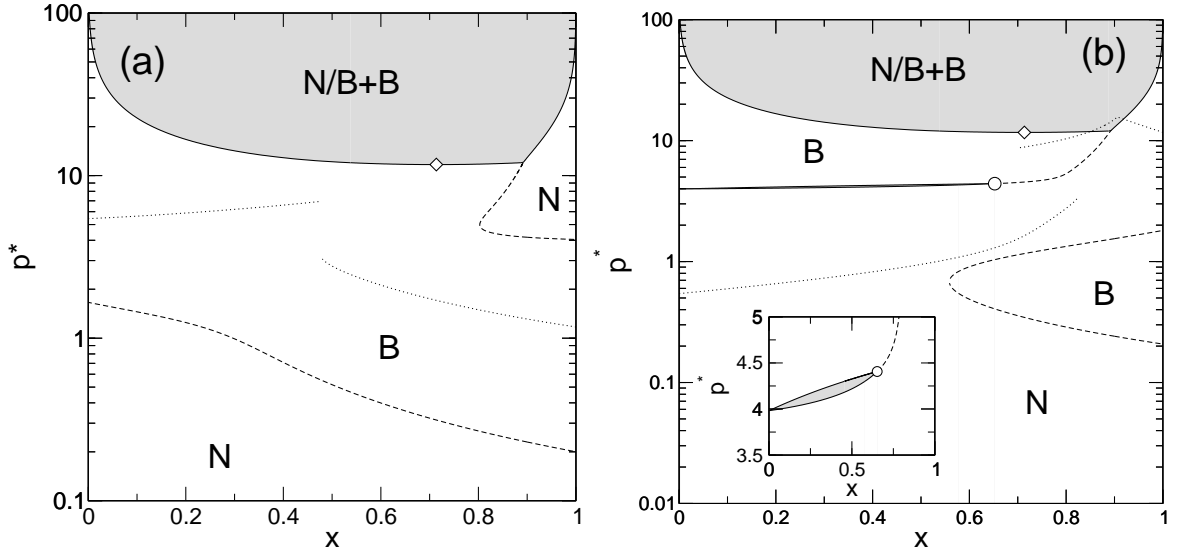


FIG. 12: Phase diagrams in the pressure-molar fraction planes corresponding to rod-plate binary mixtures with (a) $\kappa = 10$ and $(\epsilon_1, \epsilon_{-1}) = (5, 1)$, and (b) $(2, 5)$. The lines, symbols and labels have the same meaning as in Fig. 4. Inset in (b) is a zoom of the main figure showing the first-order character of the N-B transition in some pressure interval.

plate-N-B spinodal. The B phase, rich in rods, is again stable inside a island bounded by the rod-N-B spinodal. No demixing was found in this part of the phase diagram, with the N-B transition being of second order. The N/B-non-uniform-phase spinodals are now discontinuous and located above the B phase of rods.

D. Mixtures with $\kappa = 20$ and 40

The last study concerns the phase behaviour of mixtures with higher aspect ratios, in particular those with $\kappa = 20$ and 40. As shown in Fig. 13 the phase-diagram topologies are similar, but there is an important difference: now the lower tricritical point is always located below the spinodal instability to non-uniform phases. Thus there is always a range of pressures, which increases with κ , for which demixing into a N phase and a B phase rich in rods is stable. In Figs. 13 (a) and (b) the phase diagrams for $\kappa = 20$ and $(\epsilon_1, \epsilon_{-1}) = (1.5, 1.5)$, panel (a), and $(3, 1.5)$, panel (b), are shown. Note that the former mixture is symmetric with respect to adsorption. The upper boundary of the rod-N-B spinodal meets the N-B-plate spinodal at intermediate compositions. The phase behaviour includes: N-B demixing

between two tricritical points (the lower one departing from the rod-N-B spinodal), and a strongly first-order N-B transition driven by the desorption of plates, beginning at $x = 0$ and ending in a tricritical point located at the plate-N-B spinodal. This point and the upper critical point of the demixing transition are now very close to each other. An island of N-phase stability exists at high pressure as a consequence of the coalescence between the right part of the plate-N-B spinodal and the upper part of the rod-N-B spinodal. Finally, N/B-B demixing of the effective two-dimensional mixture of squares and rectangles at high pressure is also present. The phase diagram topology for the second mixture studied, that with $(\epsilon_1, \epsilon_{-1}) = (3, 1.5)$, is very similar to the for $\kappa = 10$ described before. Again there is an important difference, namely the existence of stable N-B demixing in some pressure range. Also the B phase, rich in rods, is stable in a rather large region of the phase diagram.

We end this section by showing the phase diagram of a mixture with $\kappa = 40$ and $(\epsilon_1, \epsilon_{-1}) = (1, 1)$, in Figs. 13(c) and (d). We concentrate on some details of the phase diagram topology not found before: (i) The presence of a lower critical point (at low pressures and close to the lower N-B tricritical point) above which B-B demixing takes place in a rather small range of pressures [see inset of panel (d)]. (ii) The two distinct tricritical points, located close to each other in previous cases [e.g. the case $\kappa = 20$ and $(\epsilon_1, \epsilon_{-1}) = (1.5, 1.5)$] now coalesce into a single azeotropic point [see panel (d)].

IV. CONCLUSIONS

We have systematically studied the phase behaviour of mixtures of rods and plates adsorbed on a monolayer. In our model, the particle centres of mass are taken to freely move on the surface, while particles can rotate in 3D within the restricted-orientation, Zwanzig approximation. Adsorption of the particle surfaces on the monolayer is mimicked through an attractive external potential proportional to the area of the particle surface contact, while the strengths of this interaction, $(\epsilon_1, \epsilon_{-1})$, depend on the species type. Rods and plates were taken to be symmetric, i.e. with the same volume and same aspect ratio κ . A FMT-based DF, adapted to the present constrained geometry, was minimised, and phase diagrams of mixtures with $\kappa = 10, 20$ and 40 and different values of $(\epsilon_1, \epsilon_{-1})$ were calculated.

The main results can be summarized as follows. (i) When both adsorption strengths ϵ_s are zero or small, rods and plates orient perpendicular and parallel to the surface, respectively.

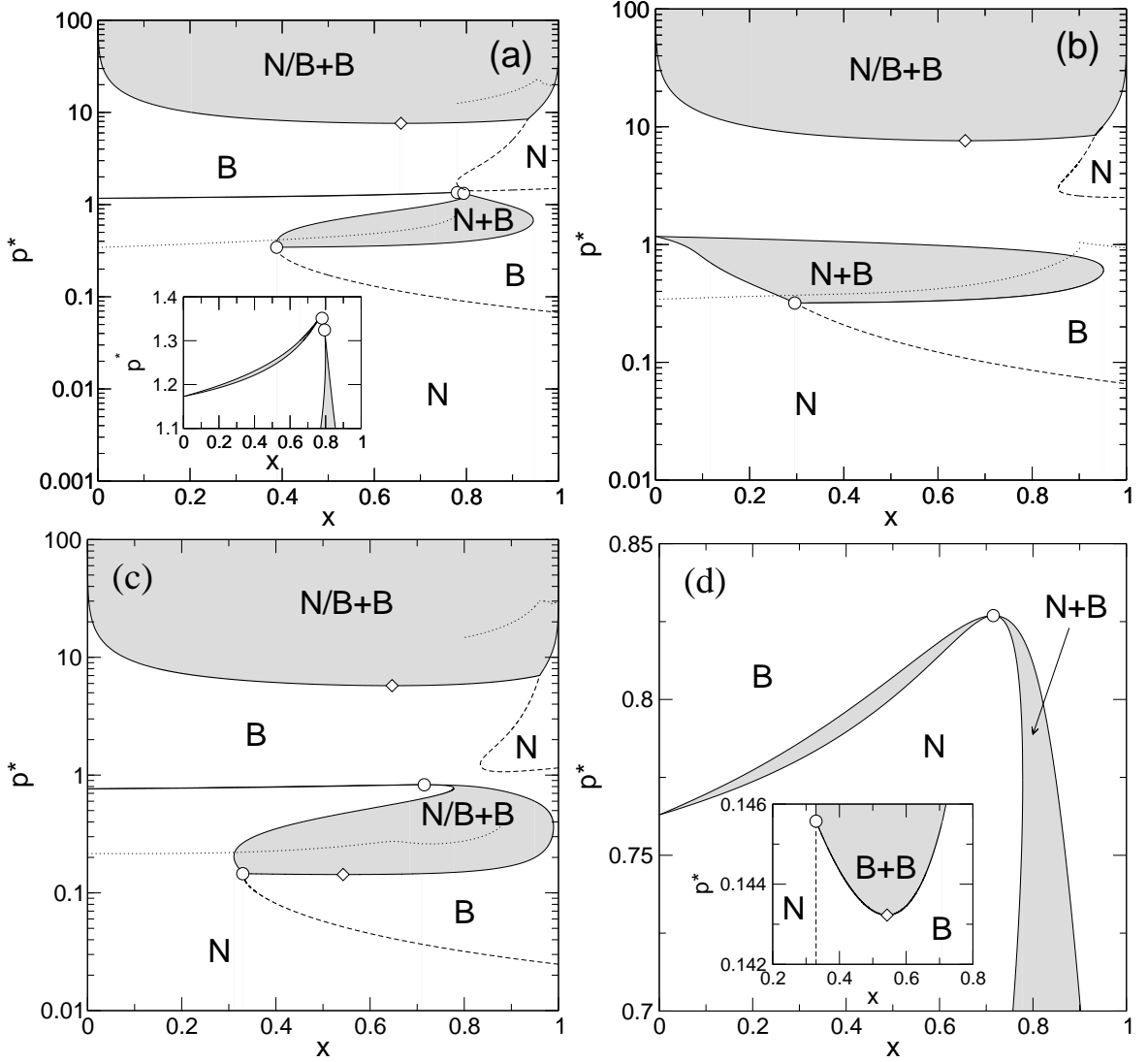


FIG. 13: Phase diagrams in the pressure-molar fraction plane of rod-plate binary mixtures for (a) $\kappa = 20$, $(\epsilon_1, \epsilon_{-1}) = (1.5, 1.5)$, (b) $\kappa = 20$, $(\epsilon_1, \epsilon_{-1}) = (3, 1.5)$, (c) and (d) $\kappa = 40$, $(\epsilon_1, \epsilon_{-1}) = (1, 1)$. The lines, symbols and labels have the same meaning as in Fig. 4 and 8. In panel (d) we show two enlarged regions of the phase diagram shown in (c): one close to the N-B azeotropic point (main figure), and the other close to the lower B-B critical point (inset).

The degree of orientation continuously increases with pressure, and at some value (which depends on the composition) a second-order N-B transition occurs, at which the plate axes orient along a director lying on the surface. Although rods also exhibit biaxial ordering, this transition is governed by the orientational symmetry breaking of plate axes, and consequently the plate-N-B spinodal is a monotonically increasing function of x . (ii) At some value of ϵ_1

and, starting at the $x = 1$ vertical axis at low pressures, there appears an island of B phase stability enclosed by a rod-N-B spinodal which is disconnected from the plate-N-B spinodal. The N-B transition is of second order and is governed by the alignment of rods with axes on the monolayer. As pressure increases rods prefer to align perpendicular to the surface, and biaxial ordering disappears. (iii) When rods and plates are symmetrically adsorbed on the monolayer ($\epsilon_1 = \epsilon_{-1}$) and the strengths are relatively large, two tricritical points appear on the rod-N-B spinodal; between these two points N-B demixing takes place, with demixed phases rich in one of the components. The B and N coexisting phases are mostly populated by rods and plates, respectively. Also, there is a strongly first-order N-B phase transition with a large density gap starting at the $x = 0$ vertical axis. This transition ends in a tricritical point located on the plate-N-B spinodal, and is driven by the desorption of the largest cross-section of the plates (corresponding to axes perpendicular to the monolayer). Finally at very high pressures, when the degree of order is high, the system effectively becomes a two-dimensional mixture of squares (the smallest projected section of rods) and rectangles (the smallest projected sections of plates), which demix into a B phase, rich in plates, and a N phase, rich in rods. This demixing transition ends in a critical point above which there exists a rather narrow B-B demixing region. (iv) When the adsorption of particles is very asymmetric and $\epsilon_1 > \epsilon_{-1}$, the lowest boundary of the rod-N-B spinodal connects with the left part of the plate-N-B spinodal, forming a monotonically-decreasing spinodal over the whole range of compositions. The N-B transition is always of second order when the adsorption of plates is small. Also the upper boundary of the rod-N-B spinodal connects with the right part of the plate-N-B-plate spinodal, forming an island of N stability. The highest pressure N/B-B demixing remains invariant. (v) When the adsorption of particles is very asymmetric and $\epsilon_{-1} > \epsilon_1$, the strongly first-order N-B transition governed by desorption of plates and their B ordering is present up to high molar fractions, while the N-B transition, governed by orientation of rods, is of second order and the N-B demixing disappear. The region of stability of the B phase (enclosed by the rod-N-B spinodal) is reduced as ϵ_1 becomes smaller.

We also calculated the spinodal instability of uniform phases with respect to density modulations with different symmetries (smectic, columnar or crystalline). We found that a B phase rich in rods is stable over a relatively large interval of pressures, while the strong N-B phase transition is always metastable. For $\kappa = 20$ and 40 there exists a range of pressures for which N-B demixing is stable. Of course N/B-B demixing at high pressure,

ending in a lower critical point, is also metastable. We note that demixing regions could be made wider if we chose shape-asymmetric mixtures (different volumes and/or different aspect ratios), and consequently the regions of N and B phase stability could be modified. Even the orientational symmetries of the demixed phases could be different for asymmetric mixtures as shown in theoretical calculations of freely-rotating rod-plate Onsager mixtures [40].

We are confident that the results presented in this work will be qualitatively similar if we remove the restricted orientation approximation and consider the free rotation of particle axes. Computer simulations of binary mixtures adsorbed on a flat monolayer could confirm this conclusion.

MC simulations of 2D mixtures of rods on a lattice show an interesting phase behavior [41]. When the aspect ratio of the longer rods is 7 there exist two I-N and N-I transitions as the density of longer rods is increased while that of the shorter rods is fixed below a certain critical density. This behavior resembles that of the present rod-plate mixture for which two N-B and B-N transitions take place at fixed composition as the pressure is increased and the adsorption strengths of rods is high enough. Thus it would be interesting to perform DFT calculations on mixtures of adsorbed rods to find the differences and similarities between monolayers and strictly 2D hard rod mixtures.

Also interesting are the similarities that the present system shares with the phase behaviour of monolayers of biaxial particles studied in [21]. In that case the phase diagrams, in the density-biaxial parameter plane, present a N-B spinodal, completely analogous to that of the present system, if we replace the biaxial parameter by molar fraction. Moreover, by increasing the aspect ratio of biaxial rods in the previous study, one obtains an island of B phase stability; a similar effect is found in the present study when adsorption strength is increased. Above a particular value for the largest aspect ratio of the biaxial particles, this island coalesces with the N-B spinodal, again a behaviour similar to the one found in the present study if the adsorption strength is increased beyond some critical value.

Additionally, we may ask ourselves how particle biaxiality would affect the present phase behaviour. If particles are biaxial, we would expect the N-B spinodal to shift to higher pressures, favouring the stabilisation of non-uniform phases. On the other hand, biaxiality would also reduce the island of B stability in the rod-rich part of the phase diagram. Finally it would also be possible that particle biaxiality reduced demixing gaps, because particle

projections become similar with biaxiality.

Appendix A: N-B bifurcation analysis

The constrained minimisation of the free-energy density with respect to the variables $\gamma_{s\nu}$ gives the following set of equations:

$$\gamma_{s\nu} = \frac{e^{-\Psi_{s\nu}}}{\sum_{\tau} e^{-\Psi_{s\tau}}}, \quad (\text{A1})$$

where

$$\Psi_{sx} = \left(\frac{n_0}{1-n_2} + \frac{n_{1x}n_{1y}}{(1-n_2)^2} - \epsilon_s \right) \kappa^{s/3} + \frac{n_{1x}\kappa^{-s/3} + n_{1y}\kappa^{2s/3}}{1-n_2}, \quad (\text{A2})$$

$$\Psi_{sy} = \left(\frac{n_0}{1-n_2} + \frac{n_{1x}n_{1y}}{(1-n_2)^2} - \epsilon_s \right) \kappa^{s/3} + \frac{n_{1x}\kappa^{2s/3} + n_{1y}\kappa^{-s/3}}{1-n_2}, \quad (\text{A3})$$

$$\Psi_{sz} = \left(\frac{n_0}{1-n_2} + \frac{n_{1x}n_{1y}}{(1-n_2)^2} - \epsilon_s \right) \kappa^{-2s/3} + \frac{(n_{1x} + n_{1y})}{1-n_2} \kappa^{-s/3}. \quad (\text{A4})$$

Using the definition of biaxial order parameter Δ_s from (9), we arrive at

$$\Delta_s = \frac{s(e^{-\Psi_{sx}} - e^{-\Psi_{sy}})}{e^{-\Psi_{sx}} + e^{-\Psi_{sy}}}, \quad s = \pm 1. \quad (\text{A5})$$

Expanding (A5) with respect to Δ_s (obviously the functions $\Psi_{s\nu}$ depend on $\{Q_s, \Delta_s\}$) up to first order gives a system of two equations which has a nontrivial solution only if the number density is such that

$$\rho^{-1} = \frac{1}{2} \sum_s x_s \kappa^{-2s/3} [(\kappa^{2s} + 1) + \gamma_{sz} (1 - \kappa^{2s})], \quad (\text{A6})$$

where γ_{sz} is the solution of (A1) for $\nu = z$, and the functions $\Psi_{s\nu}$ are calculated from (A2)-(A4), with all the weighted densities depending only on γ_{sz} , as $n_0 = \rho$ and

$$n_{1x} = n_{1y} = \frac{\rho}{2} \sum_s x_s [\kappa^{2s/3} + \kappa^{-s/3} + \gamma_{sz} (\kappa^{-s/3} - \kappa^{2s/3})], \quad (\text{A7})$$

$$n_2 = \eta = \rho \sum_s x_s [\kappa^{s/3} + \gamma_{sz} (\kappa^{-2s/3} - \kappa^{s/3})] \quad (\text{A8})$$

Thus we need to solve a system of two non-linear equations to find the equilibrium values of γ_{sz} , and consequently the number density ρ at which a bifurcation from the N to the B phase occurs.

Appendix B: Spinodal instability to non-uniform phases

We have calculated the spinodal instability of uniform phases with respect to spatial inhomogeneities through the divergence of the structure factor. The Fourier transform of the direct correlation functions, calculated through the second functional derivative of the functional, reads

$$\begin{aligned}
-\hat{c}_{s\mu,s'\nu}(\mathbf{q}) &= \frac{\langle \hat{\omega}_{s\mu}^{(0)}(\mathbf{q})\hat{\omega}_{s'\nu}^{(2)}(\mathbf{q}) + \hat{\omega}_{s\mu}^{(1x)}(\mathbf{q})\hat{\omega}_{s'\nu}^{(1y)}(\mathbf{q}) \rangle}{1 - n_2} \\
&+ \frac{\langle \left(\hat{\omega}_{s\mu}^{(1x)}(\mathbf{q})n_{1y} + \hat{\omega}_{s\mu}^{(1y)}(\mathbf{q})n_{1x} \right) \hat{\omega}_{s'\nu}^{(2)}(\mathbf{q}) \rangle}{(1 - n_2)^2} \\
&+ \left(\frac{n_0}{(1 - n_2)^2} + \frac{2n_{1x}n_{1y}}{(1 - n_2)^3} \right) \hat{\omega}_{s\mu}^{(2)}(\mathbf{q})\hat{\omega}_{s'\nu}^{(2)}(\mathbf{q}), \tag{B1}
\end{aligned}$$

where $\langle f_{s\mu,s'\nu} \rangle = f_{s\mu,s'\nu} + f_{s'\nu,s\mu}$ implies symmetrisation with respect to the pair of indexes $(s\mu, s'\nu)$, and the weighted densities n_α correspond to the stable uniform N or B phases, with orientational order parameters calculated from the minimisation of the corresponding free energies. The Fourier transforms of the weighting functions are

$$\hat{\omega}_{s\mu}^{(0)}(\mathbf{q}) = \chi_0(q_x\sigma_{s\mu}^x/2)\chi_0(q_y\sigma_{s\mu}^y/2), \quad \hat{\omega}_{s\mu}^{(2)}(\mathbf{q}) = \sigma_{s\mu}^x\sigma_{s\mu}^y\chi_1(q_x\sigma_{s\mu}^x/2)\chi_1(q_y\sigma_{s\mu}^y/2), \tag{B2}$$

$$\hat{\omega}_{s\mu}^{(1x)}(\mathbf{q}) = \sigma_{s\mu}^x\chi_1(q_x\sigma_{s\mu}^x/2)\chi_0(q_y\sigma_{s\mu}^y/2), \quad \hat{\omega}_{s\mu}^{(1y)}(\mathbf{q}) = \sigma_{s\mu}^y\chi_0(q_x\sigma_{s\mu}^x/2)\chi_1(q_y\sigma_{s\mu}^y/2), \tag{B3}$$

where $\chi_0(x) = \cos x$ and $\chi_1(x) = \sin(x)/x$. We define the 6×6 structure factor matrix

$$S_{\alpha,\beta}^{-1}(\mathbf{q}) = \delta_{ss'}\delta_{\mu\nu} - \rho_{s\mu}\hat{c}_{s\mu,s'\nu}(\mathbf{q}), \tag{B4}$$

where $\alpha = s + \mu + 1$ and $\beta = s' + \nu + 1$ if $s = -1$, and $\alpha = s + \mu + 2$ and $\beta = s' + \nu + 2$ if $s = 1$ (with the corresponding relabelling $\mu = 1, 2$ and 3 for x, y and z , respectively). Evaluating the determinant of this matrix $\mathcal{S}(q; \rho^*) \equiv \det [S_{\alpha,\beta}^{-1}(q)]$ at the wave vectors $\mathbf{q} = (0, q)$ or $\mathbf{q} = (q, 0)$ (corresponding to inhomogeneities along or perpendicular to the nematic director, respectively), we found the corresponding values at the spinodal instabilities, q_s and ρ_s^* , as the values for q and ρ^* where the absolute minimum of $\mathcal{S}(q; \rho^*)$ as a function of q becomes zero for the first time. This is equivalent to solving the pair of equations

$$\mathcal{S}(q; \rho^*) = 0, \quad \frac{\partial \mathcal{S}}{\partial q}(q; \rho^*) = 0. \tag{B5}$$

Acknowledgments

We acknowledge financial support from Grants FIS2013-47350-C5-1-R and FIS2015-66523-P from Ministerio de Economía y Competitividad of Spain.

- [1] P. Sharma, A. Ward, T. Gibaud, M. F. Hagan, and Z. Dogic, *Nature* **513**, 77 (2014).
- [2] P. A. Rice and H. M. McConnell, *Proc. Natl. Acad. Sci. USA* **86**, 6445 (1989).
- [3] J. P. Hagen and H. M. McConnell, *BBA-Biomembranes* **1329**, 7 (1997).
- [4] S. L. Keller, W. H. Pitcher III, W. H. Huestis, and H. M. McConnell, *Phys. Rev. Lett.* **81**, 5019 (1998).
- [5] S. L. Keller, and H. M. McConnell, *Phys. Rev. Lett.* **82**, 1602 (1999).
- [6] S. Baukina, E. Mendez-Villuendas, and D. Peter Tielemann, *J. Am. Chem. Soc.* **134**, 17543 (2012)
- [7] J. Zanghellini, F. Wodeli, and H. H. von Grünberg, *J. Theor. Biol.* **264**, 952 (2010).
- [8] H. E. Ries Jr., and D. C. Walker, *J. Coll. Sci. Imp U Tok* **16**, 361 (1961).
- [9] R. K. Smith, S. M. Reed, et. al., *J. Phys. Chem. B* **105**, 1119 (2001).
- [10] T. Martynski, R. Hertmanowski, and D. Bauman, *Liq. Cryst.* **28**, 2001.
- [11] H. Müller, R. Zentel, A. Janshoff, and M. Janke, *Langmuir* **22**, 11034 (2006).
- [12] I. Kalashnikova, H. Bizot, P. Bertoncini, B. Cathala, and I. Capron, *Soft Matter* **9**, 952 (2013).
- [13] D. Kim, W. D. Kim M. S. Kang, S. H. Kim, D. C. Lee, *Nano Letters* **15**, 714 (2015).
- [14] E. Kim, K. Stratford, R. Adhikari, and M. E. Cates, *Langmuir* **24**, 6549 (2008).
- [15] S. R. Vora, B. Bognet, H. S. Patanwala, F. Chinesta, A. W. K. Ma, *Langmuir* **31**, 4663 (2015).
- [16] G. B. Davies, T. Krüger, P. V. Coveney, J. Harting, and F. Bresme, *Adv. Mater.* **26**, 6715 (2014).
- [17] A. N. Sekar Iyengar, A. Datta, and M. S. Jakani, *Phys. Rev. E* **92**, 032907 (2015).
- [18] J. A. Cuesta and Y. Martínez-Ratón, *Phys. Rev. Lett.* **78**, 3681 (1997).
- [19] Y. Martínez-Ratón, *Phys. Rev. E* **69**, 061712 (2004)
- [20] Y. Martínez-Ratón, S. Varga, and E. Velasco, *J. Chem. Phys.* **140**, 204906 (2014).
- [21] M. González-Pinto, Y. Martínez-Ratón, E. Velasco, and S. Varga, *Phys. Chem. Chem. Phys.* **17**, 6389 (2015).

- [22] S. Varga, Y. Martínez-Ratón, E. Velasco, G. Bautista-Carbajal, and G. Odriozola, *Phys. Chem. Chem. Phys.* **18**, 4547 (2016).
- [23] T. Heinemann, M. Antlanger, M. Mazars, S. H. L. Klapp, and G. Kahl, *J. Chem. Phys.* **144**, 074504 (2016).
- [24] L. J. Yu and A. Saupe, *Phys. Rev. Lett.* **45**, 1000 (1980).
- [25] L. A. Madsen, T. J. Dingemans, M. Nakata and E. T. Samulski, *Phys. Rev. Lett.* **92**, 145505 (2004).
- [26] B. R. Acharya, A. Primak and S. Kumar, *Phys. Rev. Lett.* **92**, 145506 (2004).
- [27] Y. Galerne, *Phys. Rev. Lett.* **96**, 219803 (2006).
- [28] L. A. Madsen, T. J. Dingemans, M. Nakata and E. T. Samulski, *Phys. Rev. Lett.* **96**, 219804 (2006).
- [29] E. van den Pol, A. V. Petukhov, D. M. E. Thies-Weesie, D. V. Byelov and G. J. Vroege, *Phys. Rev. Lett.* **103**, 258301 (2009).
- [30] B. G. M. Leferink op Reinink, S. Belli, R. van Roij, M. Dijkstra, A. V. Petukhov and G. J. Vroege, *Soft Matter* **10**, 446 (2014).
- [31] R. Berardi, L. Muccioli, S. Orlandi, M. Ricci, and C. Zannoni, *J. Phys.: Condens. Matter* **20**, 463101 (2008).
- [32] G. Jan Vroege, *Liq. Cryst.* **41**, 342 (2013).
- [33] *Biaxial nematic liquid crystals, theory, simulation and experiment*, G. R. Luckhurst and T. J. Sluckin (eds.), Wiley (2015).
- [34] R. van Roij and B. Mulder, *J. Phys. II France* **4**, 1763 (1994).
- [35] S. Varga, A. Galindo, and G. Jackson, *Phys. Rev. E* **66**, 011707 (2002).
- [36] S. Varga, A. Galindo, and G. Jackson, *J. Chem. Phys.* **117**, 10412 (2002).
- [37] Y. Martínez-Ratón, and J. A. Cuesta, *Phys. Rev. Lett.* **89**, 185701 (2002).
- [38] Y. Martínez-Ratón, and J. A. Cuesta, *J. Chem. Phys.* **118**, 10164 (2003).
- [39] M. Oettel, M. Klopotek, M. Dixit, E. Empting, T. Schilling, and H. Hansen-Goos, [arXiv:1605.02903](https://arxiv.org/abs/1605.02903) (2016).
- [40] H. H. Wensink, G. J. Vroege, and H. N. W. Lekkerkerker, *Phys. Rev. E* **66**, 041704 (2002).
- [41] J. Kundu, J. Stilck, and R. Rajesh, *EPL* **112** 66002 (2015).